Journal of Materials Chemistry B

ROYAL SOCIETY OF CHEMISTRY

PAPER

Polar ammoniostyryls easily converting a clickable lipophilic BODIPY in an advanced plasma membrane probe†

Cite this: DOI: 10.1039/d2tb02516g

Sergio Serrano-Buitrago,[a] Mónica Muñoz-Úbeda,[bc] Víctor G. Almendro-Vedia,[bd] Juan Sánchez-Camacho,[a] Beatriz L. Maroto,[a] Florencio Moreno,[a] Jorge Bañuelos,[e] Inmaculada García-Moreno,[f] Iván López-Montero *[bcg] and Santiago de la Moya *[a]

Received 17th November 2022,
Accepted 12th February 2023

DOI: 10.1039/d2tb02516g

rsc.li/materials-b

A very simple, small and symmetric, but highly bright, photostable and functionalizable molecular probe for plasma membrane (PM) has been developed from an accessible, lipophilic and clickable organic dye based on BODIPY. To this aim, two lateral polar ammoniostyryl groups were easily linked to increase the amphiphilicity of the probe and thus its lipid membrane partitioning. Compared to the BODIPY precursor, the transversal diffusion across lipid bilayers of the ammoniostyryled BODIPY probe was highly reduced, as evidenced by fluorescence confocal microscopy on model membranes built up as giant unilamellar vesicles (GUVs). Moreover, the ammoniostyryl groups endow the new BODIPY probe with the ability to optically work (excitation and emission) in the bioimaging-useful red region, as shown by staining of the plasma membrane of living mouse embryonic fibroblasts (MEFs). Upon incubation, this fluorescent probe rapidly entered the cell through the endosomal pathway. By blocking the endocytic trafficking at 4 °C, the probe was confined within the PM of MEFs. Our experiments show the developed ammoniostyrylated BODIPY as a suitable PM fluorescent probe, and confirm the synthetic approach for advancing PM probes, imaging and science.

1. Introduction

The formation, differentiation and reorganization of the plasma membrane (PM) constitute a motley set of complex and dynamic processes which are fundamental for cell survival and division, and therefore for Life.[1] Moreover, beyond its basic function as the cell barrier and container, PM plays key roles in cell signaling and trafficking, cellular uptake, muscle contraction or neuronal communication, among other important functions.[2] In fact, PM dysfunctions are usually associated to important pathologies such as cancer.[3–5] However, despite the fundamental importance of PM in health and disease, and the impressive advances in PM knowledge,[6] deeper insights are still required.[7]

To advance the knowledge on PM processes, PM imaging by fluorescence microscopy is fundamental due to biocompatibility and spatial-temporal resolution.[8] However, PM imaging is limited by the availability, efficiency and high cost of the currently-established PM fluorescent probes.

Against the big and expensive PM probes based on fluorescent bioconjugates, such as the popular fluorescently labeled lectins, including wheat germ agglutinin (WGA), simpler PM molecular probes exhibit significant advantages related to their small size.[9–11] This size, within the scale of the PM lipids, results pivotal to conduct accurate bioimaging experiments based on the precise distribution of the probe in the PM lipidic bilayer (*e.g.*, to efficiently detect PM proteins by Förster resonance energy transfer from the probe, or to track PM microdomains by super-resolution imaging).[12–16] Moreover,

[a] *Departamento de Química Orgánica, Facultad de Ciencias Químicas, Universidad Complutense de Madrid, Ciudad Universitaria s/n, 28040, Madrid, Spain*
[b] *Instituto de Investigación Biomédica Hospital Doce de Octubre (imas12), Avda. de Córdoba s/n, 28041, Madrid, Spain*
[c] *Departamento de Química Física, Facultad de Ciencias Químicas, Universidad Complutense de Madrid, Ciudad Universitaria s/n, 28040, Madrid, Spain*
[d] *Departamento de Farmacia Galénica y Tecnología de los Alimentos, Facultad de Veterinaria, Universidad Complutense de Madrid, Ciudad Universitaria s/n, 28040, Madrid, Spain*
[e] *Departamento de Química Física, Facultad de Ciencia y Tecnología, Universidad del País Vasco (UPV-EHU), Barrio Sarriena s/n, 48080, Bilbao, Spain*
[f] *Departamento de Química-Física de Materiales, Instituto de Química Física Rocasolano, C.S.I.C., 28006, Madrid, Spain*
[g] *Instituto Pluridisciplinar, Universidad Complutense de Madrid, Paseo de Juan XXIII 1, 28040, Madrid, Spain*

† Electronic supplementary information (ESI) available: Synthetic procedures, NMR spectra of new compounds photophysical and characterization data, as well as Fig. S1–S3 and Tables S1. See DOI: **https://doi.org/10.1039/d2tb02516g**

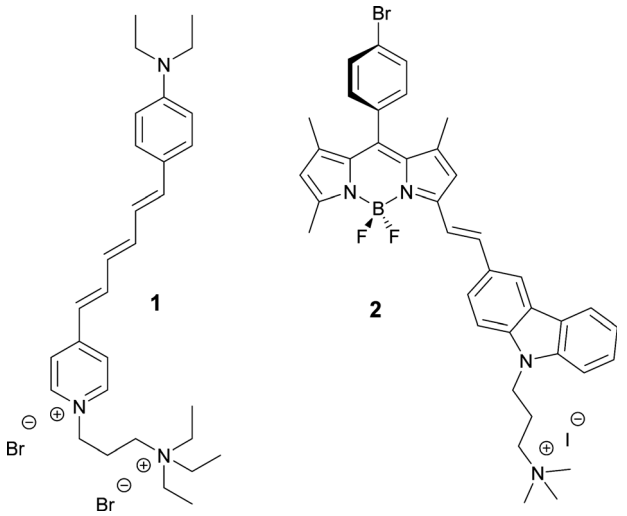

Fig. 1 Commercially available PM probe FM 4–64 (**1**) and Xiao's BODIPY-based PM probe **2**.

fluorescent bioconjugates are known to strongly participate in the cell biology due to their own pseudo-biological nature, increasing artifacts by undesired interactions with the studied biological system.[17] Unfortunately, despite their interest for PM knowledge, including neuroscience, efficient PM molecular probes are still scarce, due to the difficulties of an effective design to gain PM specificity.

Thus, although a number of lipophilic small fluorophores are known to efficiently mark lipid membrane models (*e.g.*, liposomes or giant unilamellar vesicles, GUVs), they fail to efficiently probe PM. The reason is their tendency to quickly cross the PM, staining cell inner membranes (*e.g.*, endoplasmatic reticulum) and other lipid-rich cell systems (*e.g.*, lipid droplets).[15,18] Nonetheless, some clever approaches and rational organic chemistry have allowed the development of a battery of amphiphilic-enough small fluorophores able to act as PM molecular probes by enhanced membrane fixation,[19–22] such as the commercial cyanine-like FM dyes (*e.g.*, **1** in Fig. 1)[9–11] or the panchromatic *MemBright* family of carbocyanine-based dyes developed by Collot, Danglot and Krimchenko.[21] These dyes proved to successfully mark PM and paved the way for revealing the dynamics of interesting PM processes. Unfortunately, poor fluorescent brightness, limited long-term signaling, high dependence of the probe's optical signatures with the media, large fwhm (full width at half maximum) emission, and high tendency to aggregate in aqueous media are common drawbacks of most of them.[23–25] In this scenario, the synthetic development of simpler, more robust and more efficient PM molecular probes are highly sought-after.

To offset the above mentioned shortcomings, Xiao's group cleverly took advantage of the excellent chemical and photophysical features (easy synthesis and modification, and excellent photonic efficiency) of the BODIPY (boron dipyrromethene) chromophore to develop a structurally-simple red-emitting PM molecular probe (**2** in Fig. 1).[25] However, the synthetic development of this probe is still too tedious, and it involves a number of non-commercial precursors and intermediates of different nature (BODIPYs and aldehydes). Besides, the lack of reactive-enough functional groups in its structure makes it difficult to easily tune its chemical and (bio)photophysical properties. Regarding the latter, Collot, Klimchenko *et al.* have demonstrated the advantage of having a reactive an alkynyl group to easily tune key properties (*e.g.*, amphiphilicity) in PM probes, including BODIPY-based ones, by workable click chemistry.[21,26,27]

On the basis of all the above exposed, we came interested in the development of a new PM fluorescent molecular probe which was, at the same time, structurally simple and highly efficient.

2. Materials and methods

2.1. Chemistry

Anhydrous solvents were prepared by distillation over standard drying agents according to common methods. All other solvents were of HPLC grade and were used as provided. Starting chemical substrates and reagents were used as commercially provided. Thin-layer chromatography (TLC) was performed on silica gel plates, and the chromatograms were visualized using UV light (λ = 254 or 365 nm). Flash column chromatography was performed using silica gel (230–400 mesh).

2.2. Structural characterization

^{1}H and ^{13}C NMR spectra were recorded in MeOH-d_4 solution at 20 °C. NMR chemical shifts are expressed in parts per million (δ scale) downfield from tetramethylsilane and are referenced to the corresponding residual signals of MeOH-d_4 (δ = 3.310 ppm in ^{1}H and 49.000 ppm in ^{13}C NMR). Signal pattern is indicated as follows: s = singlet, d = doublet, t = triplet, q = quartet, m = multiplet and/or multiple resonances, and br = broad. Coupling constants (J) are expressed in hertz (Hz). The type of carbon (C, CH, CH_2 or CH_3) was determined by DEPT-135 NMR experiments. Complex spin-system signals were simulated by using MestRe-C (Cobas, C. Cruces, J. Sardina, J., MestRe-C program version 2.3). FTIR spectra were recorded from neat samples using the attenuated total reflection (ATR) technique. High-resolution mass spectrometry (HRMS) was performed using electrospray ionization and hybrid quadrupole time-of-flight mass analyser (QTOF; positive- or/and negative-ion mode).

2.3. Photophysical characterization

UV-Vis absorption and fluorescence spectra were recorded on a Varian (model CARY 4E) spectrophotometer and an Edinburgh Instrument spectrofluorometer (model FLSP 920), respectively, from diluted dye solutions (*ca.* 2 μM). These solutions were prepared from a concentrated stock solution in methanol (*ca.* 10^{-3} M), by solvent evaporation of the corresponding aliquot under reduced pressure and subsequent dilution with the desired solvent of spectroscopic grade. Owing to the near infrared emission of commercial probe **1**, an InGaAs detector

was used for the detection of its whole emission band. Fluorescence quantum yields (ϕ) were determined from corrected spectra (detector sensibility to the wavelength) by the optically dilute relative method and by using eqn (1), where A_{exc} is the absorbance at the excitation wavelength, $\int I d\lambda$ is the numerically integrated luminescent intensity from the luminescence spectra, and n is the index of refraction of the solution. The subscripts R and S denote reference and sample, respectively. Styryl-based dye LDS 722 (ϕ = 0.08, purchased by Exciton) and cresyl violet (ϕ = 0.54, purchased by Exciton),[28] both in methanol, were used as references for dyes **1** and **4**, respectively. The reported ϕ values are the average of, at least, five independent measurements.

$$\frac{\phi_S}{\phi_R} = \left(\frac{\int I_S d\lambda}{\int I_R d\lambda}\right)\left(\frac{A_{R,exc}}{A_{S,exc}}\right)\left(\frac{n_S}{n_R}\right)^2 \quad (1)$$

Since the aforementioned spectrofluorometer is also equipped with a wavelength-tuneable pulsed Fianium laser. The time Correlated Single-Photon Counting (TCSPC) technique was used to record the fluorescence decay curves. Fluorescence emission was monitored at the maximum emission wavelength after excitation by the said Fianium at the maximum absorption wavelength. The fluorescence lifetime (τ) was obtained from the slope of the exponential fit of the decay curve, after the deconvolution of the instrumental response signal (recorded by means of a ludox scattering suspension) by means of an iterative method. The goodness of the exponential fit was controlled by statistical parameters (chi-square and the analysis of the residuals).

2.4. Photostabillity studies

Dye photostability was evaluated by monitoring the decrease in its fluorescence emission induced upon laser excitation. To this aim, dye solution in methanol was transversely pumped with 5 mJ, 8 ns FWHM pulses from the third harmonic (355 nm) of a Q-switched Nd:YAG laser (Lotis TII 2134) at a repetition rate of 10 Hz. The exciting pulses were line-focused onto the cell using a combination of positive and negative cylindrical lenses (f = 15 cm and f = −15 cm, respectively) perpendicularly arranged. Spectroscopic quartz cuvettes with 0.1 cm optical were used to allow for the minimum solution volume (40 μL) being excited. The lateral faces were grounded, whereupon no laser oscillation was obtained. The fluorescence emission was monitored perpendicular to the exciting beam, collected by an optical fiber, and imaged onto a spectrometer (Acton Research corporation) and detected with a charge-coupled device (CCD) (SpectruMM:GS128B). The fluorescence emission was recorded by feeding the signal to the boxcar (Stanford Research, model 250) to be integrated before being digitized and processed by a computer. Optically matched solutions of **1** and **4** at 355 nm were used to avoid the influence of their different absorption coefficients in the experimental data.

2.5. Electroformation of giant unilamellar vesicles

GUVs were prepared using the standard electroformation protocol using indium-tin-oxide (ITO)-covered slides.[29] As phosphatidylcholine is the most present lipid on plasma membranes,[30] GUVs were firstly prepared by transferring on each ITO slide two 5 μL drops of 1 mg mL^{-1} 1,2-palmitoyloleyl-*sn*-glycero-3-phosphocholine (POPC, Avanti Polar, Merck) dissolved on chloroform. Then, the films were rehydrated on the electroformation chamber with sucrose (Sigma Aldrich, Merck) solution (200 mM, pH 6), and the electrodes were connected to an AC power supply (10 Hz, 1.1 V Agilent) for at least 3 h at room temperature. After that, 50 μL of GUVs were transferred to an observation chamber filled with 50 μL glucose (Sigma Aldrich, Merck) solution (200 mM) and incubated with BODIPY **3** and/or BODIPY **4** at a final concentration of 200 nM for imaging.

2.6. Cell cultures preparation

Mouse embryonic fibroblasts (MEFs) (ATCC CRL-2991) were cultured in Dulbecco Modified Eagle Medium (DMEM), 25 mM glucose (Gibco) supplemented with 10% fetal bovine serum (South Africa S1300 Biowest, Nuallé, France), penicillin/streptomycin (final concentration 100 U mL^{-1} of penicillin and 100 μg mL^{-1} of streptomycin), and 1% of non-essential amino acids (all Gibco). The cells were grown in a humidified incubator (Forma Steri-Cycle Themofisher 5% CO_2) at 37 °C and maintained with a split ratio of 1 : 10 at 80% of confluence in T75 flasks (Nunc). For confocal microscopy imaging, cells were collected and seeded in a 8-chamber LabTek® slide (Thermofisher), and incubated at 37 °C to a final concentration of 10^5 cells per well. Prior to confocal fluorescence imaging, MEFs were supplemented with different probes (200 nM final concentration for BODIPY-based and FM 4–64 (Invitrogen™, Thermofisher) probes and **1** μM for tetramethylrhodamine (TMRM, T668, Invitrogen™, Thermofisher). BODIPYs **3** and **4** were dissolved in DMSO before use. Labelled MEFs were then imaged at different incubation times (0, 1, 8 and 24 h).

2.7. Confocal scanning laser microscopy

Fluorescence micrographs by confocal laser microscopy (CSLM) were collected using a Nikon Ti-E inverted microscope equipped with a Nikon C2 confocal scanning confocal module, 488 nm and 561 nm continuous lasers, emission band-pass (525/50) and long-pass (561LP) filters for the green and red channel, respectively, and a Nikon Plan Apo λ 100× 1.45 oil ∞/0.17 WD 0.13 immersion objective (commercial reference: CFI Plan Apo DM Lambda 100X Oil). To minimize undesired excitation/re-absorption effects in **4**, due to its small Stokes shift (see Fig. S1 in ESI†), this probe was excited at a wavelength lower than its maximum absorption (λ_{exc} = 561 nm *vs.* λ_{ab}^{max} = 617 nm in MeOH, see Table S1 in ESI†). Co-localization analysis was performed on whole images, or on selected regions of interest, and the corresponding Pearson's coefficient, R, was calculated with the JaCoP plug-in for ImageJ program.[31]

3. Results and discussion

We based the development of an advanced and structurally-simple PM probe on the following premises: (a) proper amphiphilicity to gain PM selectivity; (b) BODIPY chromophore for synthetic and photonic efficiency; (c) click reactivity for further probe tuning; (d) molecular simplicity towards low-cost probe. On the basis of these premises, we selected the known BODIPY **3**[32] (Fig. 2) as a possible starting candidate. Its molecular structure is extremely simple (small and symmetric), making it readily accessible from commercial precursors.[32] Moreover, it involves a highly photostable, bright and lipophilic-enough *meso*-aryl-tetramethylBODIPY core,[33] which apically carries a relatively polar propargyloxyl group. We hypothesized that this group could endow the dye with some amphiphilicity, enough to enhance its fixation in the PM, while it endows the dye with interesting clickable reactive character.

To rapidly check the ability of **3** to get fixed in the PM, we first addressed, on a qualitative basis, its amphiphilic character and its transbilayer movement after its insertion into the outer leaflet of GUVs, which were used here as a very simple PM model. BODIPY dye **3** was able to partition into lipid bilayers as shown by the brilliant green fluorescence of GUVs (Fig. 3A). However, it could not be retained in the outer leaflet of GUVs as revealed by the fluorescent staining of inner vesicles within GUVs (Fig. 3A). These results suggest a rapid flip-flop movement of **3** within the membrane, as well as certain aqueous solubility, both making the staining of the inner membranes possible.

To diminish the possible flip-flop movement of the probe, we decided to enhance its amphiphilicity by laterally implementing its molecular structure with two equal and highly polar 4-(trimethylammonio)styryl moieties, to generate BODIPY dye **4** (Fig. 2). Thus, the lateral arrangement of the polar ammonium groups in the molecular structure should diminish its possible transbilayer diffusion in lipid bilayers,[34] allowing a precise chromophoric PM targeting for accurate fluorescence microscopy experiments. This structural modification should be easily done by the well-known Knoevenagel-like chemistry of

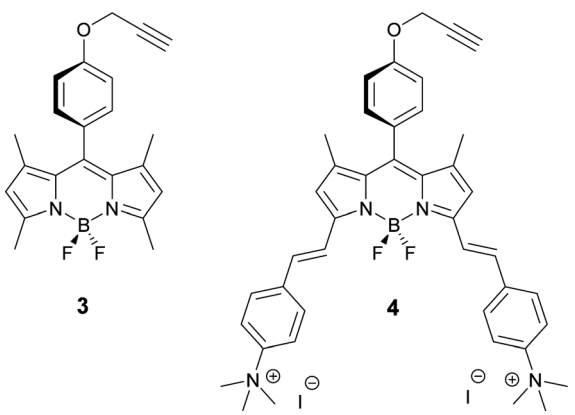

Fig. 2 Clickable, lipophilic and green-emitting BODIPY **3**, and clickable, amphiphilic and red-emitting BODIPY **4** derived from it.

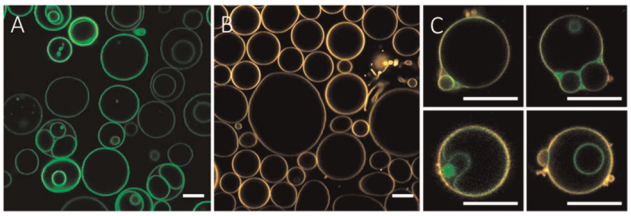

Fig. 3 (A) 1,2-Palmitoyloleyl-*sn*-glycero-3-phosphocholine (POPC) GUVs labeled with BODIPY **3**. (B) POPC GUVs labeled with BODIPY **4**. (C) Dual staining of representative POPC GUVs with BODIPY **3** and BODIPY **4**: BODIPY **3** stains outer and inner lipid bilayers, whereas BODIPY **4** exclusively labels external bilayers. GUVs were imaged after 15 minutes of incubation with probes. Final concentration of both BODIPY **3** and **4** was 200 nM. Green channel: λ_{exc} = 488 nm, λ_{em} = 525 ± 25 nm. Red channel: λ_{exc} = 561 nm, λ_{em} > 561 nm. See experimental procedures for details. Scale bars are 10 μm.

3,5-dimethyBODIPYs.[35,36] Indeed, it is known that easy distyrylation can be used to increase the hydrophilicity of highly apolar BODIPY dyes (*i.e.*, modulating the amphiphilicity), while it shifts the dye's optical signatures into the useful red-to-NIR region, as recently reported by us.[37] It must be noted here that BODIPY **4** keeps the clickable nature and the simple, symmetric structure of precursor **3** (*cf.* **3** and **4** in Fig. 2).

As expected, 3,5-distyrylated BODIPY **4** could be straightforwardly obtained from accessible 3,5-dimethylated BODIPY **3**[32] and commercially available 4-(dimethylamino)benzaldehyde in two simple synthetic steps (*ca.* 50% overall yield; see ESI† for synthetic experimental details), following the same methodology used by us for preparing related bis(ammoniostyryl)ated BODIPYs.[37]

The chemical modification implemented in BODIPY **4** resulted in a fluorescence emission spectral shift to higher wavelengths. Thus, whereas BODIPY **3** presents a maximum emission wavelength (λ_{em}) at around 515 nm in acetone,[32] the λ_{em} of BODIPY **4** shifted to 626 nm (in methanol; see Table S1 in ESI†) due to the enhanced π-extension of the involved BODIPY chromophore, and the electronic participation of the ammonium groups in it.[35] As a result, BODIPY **4** was able to label GUVs with a brilliant red fluorescence (Fig. 3B). Furthermore, unlike BODIPY **3**, BODIPY **4** remained confined to external membranes when incubated with multilamellar vesicles as revealed by dual-color experiments, where both BODIPY **3** and **4** were externally added to GUVs (Fig. 3C). The calculated Pearson's coefficient from selected regions was above threshold for external membranes, R = 0.97, whereas it dropped to R = 0.79 for inner membranes. Although these values are above the threshold value for high co-localization, they might be overestimated by the green to red bleed-through between fluorochromes, and suggest the absence of BODIPY **4** in inner membranes. These observations can be explained by the different dynamic and partitioning properties of the probes. Thus, once BODIPY **3** dyes are translocated to the inner leaflet of the external GUV, they spontaneously distribute into intraluminal vesicles because of their partial water solubility. However, BODIPY **4** remain within the outer leaflet of external GUVs

and cannot reach inner vesicles because of their negligible transversal spontaneous diffusion. The positively-charged and bulky (trimethylammonio)styryl moieties of **4** must prevent its diffusion through the hydrophobic environment of lipid bilayers.

Notably, despite its significant lipophilic character, BODIPY **4** exhibited high fluorescence quantum yield, ϕ, in hydrophilic-enough polar solvents or water (*e.g.*, ϕ = 0.68 in MeOH; see Table S1 in ESI†), supporting low chromophoric aggregation in the aqueous physiological media, an undesired common feature of the lipidic PM probes. Both the fluorescence quantum yields and the corresponding molar absorptions of **4** are significantly higher than those exhibited by the widely-used commercial PM probe FM 4–64 (**1**) under the same experimental conditions (*e.g.*, ϕ = 0.07 in MeOH for **1**; *cf.* **1** and **4** in Fig. S1 and Table S1 in ESI†). Additionally, both dyes, **1** and **4**, show similar high photostability in solution under severe laser irradiation (note that laser irradiation is used in confocal microscopy), as analyzed by the decrease of the laser-induced fluorescence (LIF) intensity with the number of pump pulses, which is almost null upon 40 000 laser pulses in both cases (see Fig. S2 in ESI†).

The fluorescence brightness, B, of BODIPY **4** in methanol ($B = \varepsilon \times \phi = 6.5 \times 10^4$ M^{-1} cm^{-1} at 626 nm, where ε is the maximum molar absorption; see Table S1 in ESI†) is slightly lower than that exhibited by Xiao's BODIPY **2** under similar conditions ($B = 8.9 \times 10^4$ M^{-1} cm^{-1} at 606 nm in ethanol, as calculated by us from previously published data;[25] see Table S1 in ESI†). Interestingly, we found the opposite behavior in water, where **4** shows fluorescence brightness two orders of magnitude higher than **2** ($B = 4.0 \times 10^2$ M^{-1} cm^{-1} for BODIPY **2** *vs.* $B = 1.2 \times 10^4$ M^{-1} cm^{-1} for **4**), due to the significant loss of fluorescence exhibited by **2** in this physiological-like medium, owing to its poor solubility in it (see Table S1 in ESI†). Additionally, **4** is red-shifted *ca.* 20 nm with respect to **2** (see Table S1 in ESI†).

All these facts support the suitability of dye **4** to act as an advanced, structurally-simple, photonically-efficient and red-working (excitation and emission) PM fluorescent molecular probe. To ground better in the ability of **4** as an efficient red PM molecular probe, we studied its performance in PM bioimaging of living mouse embryonic fibroblast (MEF) cells, in comparison with the commercially available FM 4–64 probe (**1**), which was selected for this purpose due to its wide use as an endocytosis tracer.[38] Confocal Laser Scanning Microscopy (CLSM) studies were performed to qualitatively characterize the trafficking properties of BODIPY dye **4** after its insertion into the outer leaflet of MEFs, specifically with respect to its uptake by the endocytic route. This approach also allowed us to assess through visual inspection that **4** did not provoke an apparent cell damage in the operating concentrations required for CLSM imaging (200 nM; see experimental procedures in the Materials and Methods section).

When MEFs were incubated at 37 °C with the red BODIPY probe **4**, their PMs became highly fluorescent, and this fluorescent signaling rapidly reached intracellular compartments after their internalization through the endocytic trafficking (Fig. 4A). Interestingly, MEFs remained labeled for 24 h after the addition of the probe. In contrast, the FM 4–64 probe (**1**) barely revealed the PM or the intracellular membranes when incubated at similar concentration and times, and imaged with the same acquisition settings (Fig. 4B). This observation agrees with the 10-fold-higher fluorescent quantum yield of BODIPY **4** with respect to **1** (see Table S1 in ESI†). As temperature is a crucial environmental factor that impacts drastically on endocytosis, additional experiments were run at 4 °C. At this temperature, endocytosis is negligible. When MEFs were kept at such low temperature, no labeling of intracellular compartments could be imaged even after 8 h of incubation (Fig. 4C). Surprisingly, BODIPY **4** displayed noticeable fluorescence intensity fluctuation as a function of time (Fig. 4). The absence of flip-flop of BODIPY **4** in lipid bilayers (Fig. 3C) suggests that the fluorescent probe molecules were firstly confined in the outer leaflet of PM and then internalized through the endocytic pathway. As the fluorescent probes were not washed before imaging, a sudden accumulation of **4** within the plasma membrane at short incubation times might induce the fluorescence self-quenching of the probe by chromophoric aggregation in the PM. Upon membranes recycling during 24 h, the probe redistributes reaching other compartments and recovering its initial brightness. This suggests an optimal working concentration for BODIPY probe **4** below the 0.1 μM range. All these findings demonstrate the capability of the red BODIPY dye **4** to act as a readily accessible, selective and efficient PM molecular probe, able to compete with well-known established ones.

To further consolidate the temperature-dependent data, dual-color experiments were performed at 4 °C using green BODIPY **3** and red BODIPY **4** simultaneously. As expected, the time scale and the intracellular labeling pattern were very

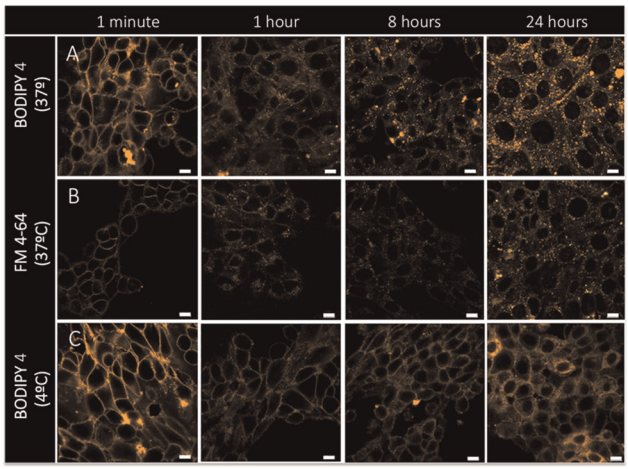

Fig. 4 Confocal fluorescence micrographs of MEFs incubated with 200 nM of BODIPY **4** (A and C) and FM 4–64 (**1**) (B). At 37 °C (A and B), both BODIPY **4** and FM 4–64 (**1**) stain the plasma membrane and rapidly reach inner cell membranes through endosomal trafficking. At 4 °C, BODIPY **4** remains within the plasma membrane for several hours. Red channel: λ_{exc} = 561 nm, λ_{em} > 561 nm. See main text for details. Scale bars are 10 μm.

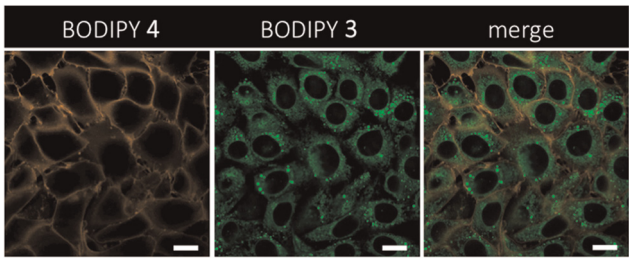

Fig. 5 Dual-color imaging of MEFs with BODIPY **4** (left), BODIPY **3** (middle) and merged channels (right). BODIPY **4** stains the plasma membrane of MEFs whereas BODIPY **3** labels inner cell membranes. Probes were incubated at 4 °C and imaged immediately after their addition. Final concentration of both BODIPY **3** and **4** was 200 nM. Green channel: λ_{exc} = 488 nm, λ_{em} = 525 ± 25 nm. Red channel: λ_{exc} = 561 nm, λ_{em} > 561 nm. See main text for details. Scale bars are 10 μm.

dependent on the probe (Fig. 5). Right after the addition of probes to the monolayer cultures of MEFs, BODIPY **4** labeled the PM whereas BODIPY **3** penetrated rapidly into the cytosol and spread over all the cell inner biomembranes. As long as the temperature was kept at 4 °C, no labeling of intracellular organelles could be detected for BODIPY **4** even after 8 h. However, the highly diffusive BODIPY **3** was able to reach non-endocytic compartments, such as mitochondria, as shown by the labeling of the mitochondrial network. Further confirmation was obtained by independent experiments where the specific imaging of the mitochondrial network was revealed by both the BODIPY **3** and the commercial mitochondrial dye tetramethylrhodamin (TMRM) (see Fig. S3 in ESI†). Upon incubation, we observed the co-localization of both probes in some elongated mitochondria, but only some of them were singly labeled with BODIPY **3** (calculated Pearson's coefficient, R = 0.62, was above the threshold). The different labeling mechanism might be behind this observation. Unlike BODIPY **3**, the cationic and lipophilic molecule TMRM is a membrane potential-dependent fluorophore that accumulates specifically inside mitochondria as long as this potential difference is maintained. TMRM is thus a good tracker for the polarization state of mitochondria and an indicator of overall health of the cell. In contrast, BODIPY **3** stains all the inner membranes including unpolarized mitochondria.

4. Conclusions

In summary, we have rationally developed a very simple, but highly efficient red-working PM fluorescent molecular probe by properly tuning a highly bright green-emitting BODIPY dye precursor. This is easily done on the basis of workable BODIPY chemistry (distyrylation of 3,5-dimethylBODIPY) to modulate both amphiphilic character and chromophoric π-extension. The polar ammoniostyryls implemented this way are demonstrated to be key to increase the fixation of the probe into the PM, diminishing its permeation across this outer membrane. Interestingly, the presence of an apical, reactive ethynyl group in the molecular structure of the developed PM probe opens the way towards valuable further probe tuning by workable click chemistry,[26,27] as well as towards future PM decoration by click biconjugation.[39,40] Noticeable PM selectivity, easy and efficient synthetic access (low-cost probe), high photonic efficiency in the bioimaging useful red spectral region, and clickable character support BODIPY **4** as a breaking PM-probe model design for advancing both smarter PM probes and demanded PM knowledge.

Author contributions

Conceptualization, S. d. l. M.; investigation—synthesis, S. S.-B. and J. S.-C.; investigation—structural characterization, B. L. M. and F. M.; investigation—photophysics, J. B. and I. G.-M.; Investigation—biophysics, M. M.-Ú., V. G. A.-V. and I. L.-M.; funding acquisition, S. d. l. M, I. L.-M., J. B. and I. G.-M.; writing—original draft preparation, S. d. l. M. and I. L.-M., with input from all the authors; writing—review and editing, S. d. l. M., J. B. and I. L.-M. All authors have read and agreed to the published version of the manuscript.

Conflicts of interest

The authors declare no conflicts of interest.

Acknowledgements

Financial support from MICINN (PID2020-114755GB-C31, -C32 and C-33) and Basque Government (IT1639-22) is gratefully acknowledged by S. d. l. M., J. B. and I. G.-M. I. L.-M. acknowledge financial support from the Spanish Ministry of Science, Innovation and Universities through the grant PGC2018-097903-B-I00. This work was also supported by the TECNOLOGÍAS 2018 program, funded by the Regional Government of Madrid (Grant S2018/BAA-4403 SINOXPHOS-CM, to I. L-M.). S. S.-B thanks the Regional Government of Madrid for an INVESTIGO contract. M. M.-Ú. was recipient of a Sara Borrell fellowship (CD15/00190) financed by the Spanish Ministry of Health. Q4

Notes and references

1 D. A. Ammendolia, W. M. Bement and J. H. Brumell, *BMC Biol.*, 2021, **19**, 71.
2 D. Lingwood and K. Simons, *Science*, 2010, **327**, 46–50.
3 M.-Y. Wu, J.-K. Leung, C. Kam, B. Situ, Z.-J. Wu, T. Y. Chou, S. Feng and S. Chen, *Cell Rep. Phys. Sci.*, 2022, **3**, 100735.
4 S. Feng, Y. Liu, Q. Li, Z. Gui and G. Feng, *Anal. Chem.*, 2022, **94**, 1601–1607.
5 H.-Y. Kwon, R. Kumar Das, G. T. Jung, H.-G. Lee, S. H. Lee, S. N. Berry, J. K. S. Tan, S. Park, J.-S. Yang, S. Park, K. Baek, K. M. Park, J. W. Lee, Y.-K. Choi, K. H. Kim, S. Kim, K. P. Kim, N.-Y. Kang, K. Kim and Y.-T. Chang, *J. Am. Chem. Soc.*, 2021, **143**, 5836–5844.
6 D. Marguet, P.-F. Lenne, H. Rigneault and H.-T. He, *EMBO J.*, 2006, **25**, 3446–3457.

7 Y. Yu and S. H. Yoshimura, *J. Cell Sci.*, 2021, **134**, 243584.
8 J. A. Steyer and W. A. Almers, *Nat. Rev. Mol. Cell Biol.*, 2001, **2**, 268–275.
9 T. P. Foster, *Methods Mol. Biol.*, 2022, **2422**, 85–124.
10 M. Collot, S. Pfister and A. S. Klymchenko, *Curr. Opin. Chem. Biol.*, 2022, **69**, 102161.
11 Thermofischer Scientific, Tracers for Membrane Labeling, in The Molecular Probes Handbook. **https://www.thermofisher.com**.
12 D. M. Owen, D. J. Williamson, A. Magenau and K. Gaus, *Nat. Commun.*, 2012, **3**, 1256.
13 I. Ziomkiewicz, A. Loman, R. Klement, C. Fritsch, A. S. Klymchenko, G. Bunt, T. M. Jovin and D. J. Arndt-Jovin, *Cytometry, Part A*, 2013, **83**, 794–805.
14 L. M. Solanko, A. Honigmann, H. S. Midtiby, F. W. Lund, J. R. Brewer, V. Dekaris, R. Bittman, C. Eggeling and D. Wüstner, *Biophys. J.*, 2013, **105**, 2082–2092.
15 A. S. Klymchenko and R. Kreder, *Chem. Biol.*, 2014, **21**, 97–113.
16 A. Honigmann, V. Mueller, H. Ta, A. Schoenle, E. Sezgin, S. W. Hell and C. Eggeling, *Nat. Commun.*, 2014, **5**, 5412.
17 S. M. Usama, E. R. Thapaliya, M. P. Luciano and M. J. Schnermann, *Curr. Opin. Chem. Biol.*, 2021, **63**, 38–45.
18 Y. Niko, P. Didier, Y. Mely, G. Konishi and A. S. Klymchenko, *Sci. Rep.*, 2016, **6**, 18870.
19 G. Bondelli, G. M. Paternò and G. Lanzani, *Opt. Mater.: X*, 2021, **12**, 100085.
20 C. Liu, X. Gao, J. Yuan and R. Zhang, *TrAC, Trends Anal. Chem.*, 2020, **133**, 116092.
21 M. Collot, P. Ashokkumar, H. Anton, E. Boutant, O. Faklaris, T. Galli, Y. Mély, L. Danglot and A. S. Klymchenko, *Cell Chem. Biol.*, 2019, **26**, 600–614.
22 L. Shi, Y. Liu, K. Li, A. Sharma, K. Yu, M. S. Ji, L. Li, Q. Zhou, H. Zhang, J. S. Kim and X. Yu, *Angew. Chem., Int. Ed.*, 2020, **59**, 9962–9966.
23 M. G. Honig and R. I. Hume, *Trends Neurosci.*, 1989, **12**, 336–338.
24 Y. Wu, F. L. Yeh, F. Mao and E. R. Chapman, *Biophys. J.*, 2009, **97**, 101–109.
25 X. Zhang, C. Wang, L. Jin, Z. Han and Y. Xiao, *ACS Appl. Mater. Interfaces*, 2014, **6**, 12372–12379.
26 M. Collot, E. Boutant, M. Lehmann and A. S. Klymchenko, *Bioconjugate Chem.*, 2019, **30**, 192–199.
27 M. Collot, E. Boutant, K. T. Fam, L. Danglot and A. S. Klymchenko, *Bioconjugate Chem.*, 2020, **31**, 875–883.
28 L. Cerdán, A. Costela, I. García-Moreno, J. Bañuelos and L. López-Arbeloa, *Laser Phys. Lett.*, 2012, **9**, 426–433.
29 L. Mathivet, S. Cribier and P. F. Devaux, *Biophys. J.*, 1996, **70**, 1112–1121.
30 H. I. Ingólfsson, M. N. Melo, F. J. Van Eerden, C. Arnarez, C. A. Lopez, T. A. Wassenaar, X. Periole, A. H. De Vries, D. P. Tieleman and S. J. Marrink, *J. Am. Chem. Soc.*, 2014, **136**, 14554–14559.
31 S. Bolte and F. P. Cordelières, *J. Microsc.*, 2006, **224**, 213–232.
32 J. Park, D. Feng and H.-C. Zhou, *J. Am. Chem. Soc.*, 2015, **137**, 1663–1672.
33 A. Tabero, F. García-Garrido, A. Prieto-Castañeda, E. Palao, A. R. Agarrabeitia, I. García-Moreno, A. Villanueva, S. de la Moya and M. J. Ortiz, *Chem. Commun.*, 2020, **56**, 940–943.
34 R. Homan and H. J. Pownall, *Biochim. Biophys. Acta*, 1988, **938**, 155–166.
35 H. Lu, J. Mack, J. Yanga and Z. Shen, *Chem. Soc. Rev.*, 2014, **43**, 4778–4823.
36 N. Boens, B. Verbelen, M. J. Ortiz, L. Liao and W. Dehaen, *Coord. Chem. Rev.*, 2019, **399**, 213024.
37 J. Jiménez, C. Díaz-Norambuena, S. Serrano, S. C. Ma, F. Moreno, B. L. Maroto, J. Bañuelos, G. Muller and S. de la Moya, *Chem. Commun.*, 2021, **57**, 5750–5753.
38 M. A. Gaffield and W. J. Betz, *Nat. Protoc.*, 2006, **1**, 2916–2921.
39 M. D. Best, *Biochemistry*, 2009, **48**, 6571–6584.
40 R. E. Bird, S. A. Lemmel, X. Yu and Q. A. Zhou, *Bioconjugate Chem.*, 2021, **32**, 2457–2479.